PHYSICAL REVIEW A VOLUME 27, NUMBER 5 MAY 1983

Two-dimensional Gaussian core model at high temperature

Frank H. Stillinger and Thomas A. Weber
Bell Laboratories, Murray Hill, New Jersey 07974
(Received 14 September 1982)

The two-dimensional Gaussian core model in the high-temperature regime has been examined by two means: (1) exact high-temperature series, and (2) molecular-dynamics simulation. The former diverge but can be summed by Borel transforms. Evidence is offered that in the case of the mean potential energy per particle and the excess pressure that the Borel transforms are analytic throughout the complex plane. Furthermore, these transforms grow exponentially along the positive real axis at a rate which determines the fluid's freezing-point temperature. Approximate Borel transforms have been constructed which fit the simulation data adequately.

I. INTRODUCTION

Very few general methods are available for extracting exact properties from classical partition functions. Perhaps the best known is the Mayer cluster expansion[1] which for short-range intermolecular potentials yields density series for thermodynamic properties of the gas phase. Low-temperature expansions can also be generated, provided that the structure of the lowest-energy crystal is known.[2] To these methods could be added the high-temperature expansions that can, in principle, be developed if the intermolecular potentials are bounded. Heretofore such high-temperature expansions have had limited application, due to the fact that they are inevitably divergent series.

The present paper is devoted to a study of the two-dimensional Gaussian core model,[3,4] particularly in its high-temperature regime. This classical model is defined by its intermolecular potential function, which in reduced units has the simple form

$$\Phi = \sum_{i<j} \exp(-r_{ij}^2) \, . \tag{1.1}$$

We examine below the high-temperature expansions for this model, and compare predictions based on those asymptotic series with results from molecular-dynamics computer simulation.

At absolute zero temperature the crystal structures and their energies have previously been determined for the Gaussian core model.[5,6] In one dimension ($D=1$) the regular linear array is the lowest-energy structure, while for $D=2$ the structure is the usual triangular close-packed crystal. When $D=3$, the structure is fcc at low density, and bcc at high density.

Owing to the fact that the Gaussian function is self-dual under Fourier transformation, the lattice energies of these $T=0$ arrays satisfy a high-density, low-density duality relation[7] for any integer D. Specifically, let

$$I = 1 + \lim_{N\to\infty} (2\Phi/N) \, , \tag{1.2}$$

where the limit is carried out for the $T=0$ array at fixed density. If high (ρ_h) and low (ρ_l) densities are chosen so that

$$\rho_h \rho_l = \pi^{-D} \, , \tag{1.3}$$

one then has the duality relation

$$\rho_h^{-1/2} I(\rho_h) = \rho_l^{-1/2} I(\rho_l) \, . \tag{1.4}$$

The analysis which produces the duality relations has an important implication, namely, that energy differences between alternative particle packings must vanish as density increases to infinity. This causes the melting temperature to pass through a maximum versus density, and to decline to zero in the infinite density limit. On the high-density side of the melting-point maximum the Clapeyron equation requires that the fluid phase be denser than the solid with which it coexists.

Molecular-dynamics simulations for the two-dimensional Gaussian core model at reduced density

$$\rho^* = 3^{-1/2} \tag{1.5}$$

have previously been reported.[3,4] That work examined a system of 780 particles in a nearly square system [side ratio $(15/26)3^{1/2}$] to which periodic boun-

dary conditions applied. The results obtained indicated a solid-fluid coexistence range in reduced temperature as follows:

$$6.6\times10^{-3}\leq T^*\leq 7.2\times10^{-3}\ . \tag{1.6}$$

Furthermore, the density shown in Eq. (1.5) at which these simulations were carried out was clearly larger than that giving the maximum melting temperature. One of the objectives of the present work has been to extend the earlier simulation study to include the very high-temperature regime where the system behaves as a weakly perturbed ideal gas.

Section II discusses the $D=2$ high-temperature expansions, indicating how the Borel transform provides the means to sum those divergent series. This is followed in Sec. III by presentation of some new molecular-dynamics results. Section IV discusses one approach to fitting the molecular-dynamics data with series-consistent Borel transforms.

II. HIGH-TEMPERATURE SERIES

The exact high-temperature asymptotic expansion for the Helmholtz free energy of the Gaussian core model has previously been calculated through eighth order,[8] with coefficients that are available as arbitrary functions of D and ρ^*. The series may be displayed in the following form:

$$\beta f(\beta,\rho_D) \sim b_{12}(D)\rho_D\beta-\sum_{n=2}^{\infty}\left[\sum_{j=2}^{n} b_{nj}(D)\rho_D^{j-1}\right](-\beta)^n\ . \tag{2.1}$$

Here f stands for the excess Helmholtz free energy per particle (in the infinite-system limit), and

$$\beta=1/T^*=1/k_BT\ ,$$
$$\rho_D=\pi^{D/2}\rho^*\ . \tag{2.2}$$

Explicit expressions for b_{nj} appear in Table I of Ref. 8; these quantities are always positive.

For present purposes we will be concerned with high-temperature series for the potential energy per particle ϕ, and the excess pressure p_{ex}, that can be obtained from Eq. (2.1) by differentiation:

$$\phi=\left[\frac{\partial[\beta f(\beta,\rho_D)]}{\partial\beta}\right]_{\rho_D,D}\sim\sum_{n=0}^{\infty}A_n(-\beta)^n\ ; \tag{2.3}$$

$$\pi^{D/2}\frac{p_{ex}}{\rho_D}=\rho_D\left[\frac{\partial f(\beta,\rho_D)}{\partial\rho_D}\right]_{\beta,D}\sim\sum_{n=0}^{\infty}C_n(-\beta)^n\ . \tag{2.4}$$

TABLE I. High-temperature series coefficients for the Gaussian core model with $D=2$ and $\rho^*=3^{-1/2}$.

n	A_n	C_n
0	0.906 899 6821	0.906 899 6821
1	0.453 449 8411	0.226 724 9205
2	0.699 461 3026	0.415 924 2194
3	1.441 656 205	0.897 855 0034
4	3.540 660 443	2.247 268 627
5	9.774 323 697	6.261 573 848
6	29.366 392 38	18.900 844 47
7	94.164 168 51	60.735 717 05

Table I presents numerical values for coefficients A_n and C_n in the cases of interest, $D=2$ and $\rho^*=3^{-1/2}$.

Figure 1 shows the ratios A_n/A_{n-1} and C_n/C_{n-1} of successive series coefficients from Eqs. (2.3) and (2.4), plotted against n. At least for the orders shown these ratios appear to converge toward one another and to rise monotonically with n. The pattern is similar to that observed for the Gaussian core-model series for the free energy itself when $D=3$.[8] Presuming that this trend continues to all orders, the ratio test[9] indicates that the series are divergent. The source of these divergences is clear: Changing the sign of β from positive to negative is tantamount to changing particle potentials from repulsive to attractive, thereby making the system unstable with respect to collapse. Consequently $\beta=0$ is expected to be a singular point. As suggested earlier the formal f, ϕ, and p_{ex} series then will only be asymptotic series.

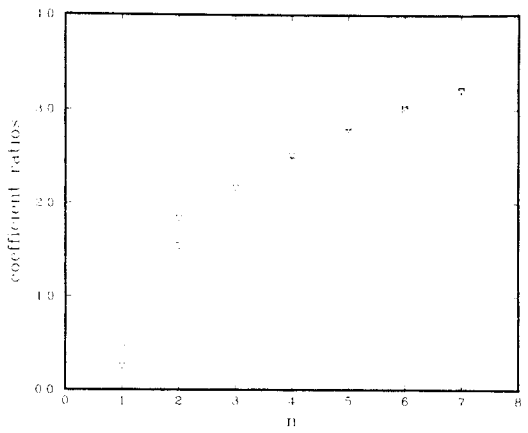

FIG. 1. Ratios of successive series coefficients plotted against order n. Squares show A_n/A_{n-1} from Eq. (2.3) and the inverted triangles show C_n/C_{n-1} from Eq. (2.4).

The Borel transform[8] appears to offer the analytical tool required to connect the asymptotic series to simulation results away from $\beta=0$. Consequently, we write

$$\phi = \int_0^\infty G(\beta t)\exp(-t)dt \ , \tag{2.5}$$

$$p_{\rm ex} = \pi^{-D/2}\rho_D \int_0^\infty H(\beta t)\exp(-t)dt \ . \tag{2.6}$$

Therefore the transform functions G and H will have the following formal power-series expansions:

$$G(x) = \sum_{n=0}^{\infty} (A_n/n!)(-x)^n \ ,$$

$$H(x) = \sum_{n=0}^{\infty} (C_n/n!)(-x)^n \ . \tag{2.7}$$

The coefficient ratios have now become $A_n/(nA_{n-1})$ and $C_n/(nC_{n-1})$; these are plotted against n in Fig. 2. Notice that beyond $n=2$ these new ratios decline with n and behave as though they converge to zero as n increases to infinity. If this pattern is indeed valid for all n then $G(x)$ and $H(x)$ will be analytic functions throughout the complex x plane.

We now revive for $D=2$ an argument previously advanced[8] which establishes the behavior of $G(x)$ for large positive real x. First, there must exist a crystallite pattern-recognition algorithm (specific details need not be of concern here), which for any system configuration partitions particles uniquely into contiguous subsets, each of which constitutes a crystallite. In particular, we will have

$$N = \sum_{l=1}^{\infty} l n_l \ , \tag{2.8}$$

where n_l is the number of l-particle crystallites present at the given instant. By default, many particles in the fluid may be so improperly coordinated that they would necessarily be consigned to the $l=1$ category, "one-particle crystallites." Nevertheless, the available pictures that have been produced from simulations of two-dimensional fluids clearly show local regions of crystalline order,[4,6,10] implying that the $l>1$ categories will not be vacant. We require of the algorithm only that it describe the fluid phase in terms of disconnected microscopic crystallites, while describing the equilibrium solid phase predominately as a single (possibly defective) macroscopic crystallite, i.e.,

$$N^{-1}\left\langle \sum_{l=1}^{N} l^2 n_l \right\rangle = \begin{cases} O(1) & \text{(fluid)} \\ O(N) & \text{(solid)} \ . \end{cases} \tag{2.9}$$

Second, consider now the equilibrium fluid phase just above its freezing point. We can denote the mean concentrations of crystallites with various sizes by $\langle n_l \rangle/\Omega$, where Ω is the content (area for $D=2$) of the system. In the large-l limit these concentrations will surely be determined by macroscopic free-energy contributions of bulk and perimetric origin. Consequently we expect to have ($k_0, k_1 > 0$)

$$\ln(\langle n_l \rangle/\Omega) \sim -k_0 l - k_1 l^{1/2} - k_2 \ln l - k_3 - \cdots \ . \tag{2.10}$$

In this expression k_0 will vanish linearly with temperature at the freezing point ($\beta=\beta_f$), while k_1 (related to the solid-fluid boundary tension) will remain greater than zero; i.e.,

$$k_0 = K_0 \Delta\beta + O((\Delta\beta)^2) \ ,$$

$$k_1 = K_1 + O(\Delta\beta) \ , \tag{2.11}$$

where K_0 and K_1 are positive constants, and

$$\Delta\beta = \beta_f - \beta \tag{2.12}$$

is positive in the fluid phase. The exponent shown for l in the second term on the right-hand side of Eq. (2.10) results from the implicit assumption that the crystallites will not be highly ramified. Essentially nothing is known about k_2 or k_3 in Eq. (2.10), but it is reasonable to assume that they approach the nonzero limits K_2 and K_3 at β_f.

Because their interiors are more ordered than the surrounding fluid, large crystallites will give anomalous negative contributions to the interaction energy of the system. More precisely we would expect that the contribution for crystallites of specific size l should have the form

$$E_l = (e_0 l + e_1 l^{1/2} + \cdots)\langle n_l \rangle \ , \tag{2.13}$$

where e_0 is negative (bulk term) and e_1 is positive (perimeter term). The entire anomalous contribution

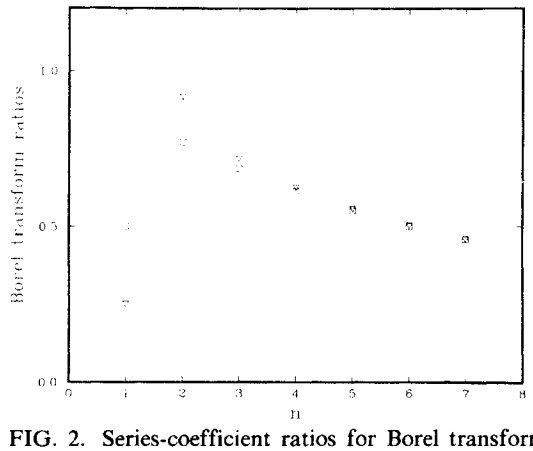

FIG. 2. Series-coefficient ratios for Borel transforms. Squares refer to G defined in Eq. (2.5), inverted triangles refer to H defined in Eq. (2.6).

attributable to crystallites can then be obtained by summing over l. The resulting function of β,

$$N\phi_{\rm cr}(\beta)=\sum_{l=1}^{\infty} E_l \ , \tag{2.14}$$

will have an essential singularity at β_f, as reference to Eqs. (2.10)–(2.13) demonstrates. This singularity stems from the accelerating rapidity, for larger and larger l, with which $\langle n_l \rangle$ increases when $\Delta\beta$ goes to zero.

The next task is to isolate in ϕ the crystallite essential singularity $\phi_{\rm cr}$. Formally we can write

$$\phi(\beta)=\phi_{\rm cr}(\beta)+\phi_a(\beta) \equiv \int_0^{\infty} [G_{\rm cr}(\beta t)+G_a(\beta t)]\exp(-t)dt \ , \tag{2.15}$$

where ϕ_a is the appropriate analytic background term, and $G_{\rm cr}$ and G_a are the respective Borel transforms. By employing Eqs. (2.10)–(2.14), we can set

$$\phi_{\rm cr}(\beta)=-\sum_{l=1}^{\infty} f_l \exp(-k_0 l - k_1 l^{1/2}) \ . \tag{2.16}$$

The quantities f_l absorb factors dominated at large l by the exponential function shown; for large l, they will be uniformly positive and are expected to vary as some power of l. It should now be possible to select a smooth function $\psi(s)$ of the continuous variable s such that, for every $l=1,2,3,\ldots$,

$$f_l \exp(-k_0 l - k_1 l^{1/2}) = \int_{l-1}^{l} \psi(s)\exp(-k_0 s - k_1 s^{1/2})ds \ . \tag{2.17}$$

Therefore

$$\phi_{\rm cr}(\beta)=-\int_0^{\infty} \psi(s)\exp(-k_0 s - k_1 s^{1/2})ds \ . \tag{2.18}$$

The function $\psi(s)$ will have the same power-law behavior for large s that f_l displays for large l.

Introducing the variable change

$$s = t/K_0\beta_f \tag{2.19}$$

in Eq. (2.18),

$$\phi_{\rm cr}(\beta)=\int_0^{\infty} \Gamma(t,\beta)\exp(-t)dt \ , \tag{2.20}$$

where

$$\Gamma(t,\beta)=-(1/K_0\beta_f)\psi(t/K_0\beta_f) \times \exp\{[1-(k_0/K_0\beta_f)]t - k_1(t/K_0\beta_f)^{1/2}\} \ . \tag{2.21}$$

When $\Delta\beta$ is small we can use Eqs. (2.11) to show that

$$\Gamma(t,\beta)=-(1/K_0\beta_f)\exp[(\beta t)/\beta_f]\{\psi[(\beta t)/K_0\beta_f^2]\exp[-(K_1/\beta_f K_0^{1/2})(\beta t)^{1/2}]+O(\Delta\beta)\} \ . \tag{2.22}$$

The terms explicitly shown here dominate the small-$\Delta\beta$ behavior of Γ, and depend only on the variable βt. They have thus the form of a Borel transform, and so we can conclude from uniqueness of the transform that this must be the form of the function $G_{\rm cr}$ in Eq. (2.15) above. Specifically, as x tends to plus infinity,

$$G_{\rm cr}(x)\sim -\exp[x/\beta_f-(K_1/\beta_f K_0^{1/2})x^{1/2} + O(\ln x)] \ . \tag{2.23}$$

Because $G_a(x)$ cannot lead to the singular behavior (at least not as strongly) as that attributable to $G_{\rm cr}$, the same asymptotic behavior must obtain for the full Borel-transform function G:

$$G(x)\sim -\exp[x/\beta_f-(K_1/\beta_f K_0^{1/2})x^{1/2} + O(\ln x)] \ . \tag{2.24}$$

The importance of this last result is that it shows how the freezing point β_f appears explicitly in G. Since the behavior of $G(x)$ near $x=0$ is connected by analytic continuation to the large-x behavior, we can say that the high-temperature expansion which determines the G power series (2.7) contains within it information about the first-order freezing transition. The Borel transform offers the means for extracting that information from the high-temperature series. We also see that, in principle, the means is at hand to extract a fluid-solid boundary free energy from the series via the coefficient of $x^{1/2}$ in Eq. (2.24).

Suppose now that the free-energy series shown in Eq. (2.1) were itself to be represented as a Borel transform (examination of its series coefficients suggests that this is appropriate):

$$f(\beta)=\int_0^{\infty} F(\beta t)\exp(-t)dt \ . \tag{2.25}$$

Clearly then

$$G(x)=[1+(d\ln F/d\ln x)]F(x) \ . \tag{2.26}$$

The only way that $G(x)$ having the asymptotic form shown earlier in Eq. (2.23) could have been generated in this way is for $F(x)$ to have a similar asymptotic representation:

$$F(x)\sim -\exp[x/\beta_f-(K_1/\beta_f K_0^{1/2})x^{1/2}+O(\ln x)] \ . \tag{2.27}$$

Only the $O(\ln x)$ part will differ between F and G.

Carrying the argument one step further, $H(x)$ can next be generated by applying a density derivative to F:

$$H(x)=\left[\frac{\partial F(x)}{\partial \ln \rho_D}\right]_{\beta,D} . \tag{2.28}$$

By referring to the asymptotic form above for F we conclude that

$$H(x)\sim[\mathrm{sgn}(\partial\beta_f/\partial\rho_D)] \times\exp[x/\beta_f-(K_1/\beta_f K_0^{1/2})x^{1/2} +O(\ln x)] . \tag{2.29}$$

Notice that the density derivative operator causes the sign of the result to depend on the way that density change affects the freezing point. As mentioned above the Gaussian core model has the interesting property that both signs can occur: At low density $\partial\beta_f/\partial\rho_D$ is negative whereas at high density it is positive.

III. MOLECULAR-DYNAMICS RESULTS

The present molecular-dynamics investigation, in the high-temperature regime with $\rho^*=3^{-1/2}$, has continued to employ a system of 780 particles. Once again the side ratio for the basic cell is $(15/26)3^{1/2}$, and periodic boundary conditions apply. Because the mean particle velocities are so much higher than before it was necessary to utilize a time increment Δt^* for numerical integration of the classical equations of motion that was only one-tenth that employed in most of our previous work[3,4,6]; in reduced units it was chosen to be

$$\Delta t^*=0.005 . \tag{3.1}$$

The final fluid configuration from the previous phase of this work[6] provided the starting particle configuration. Temperatures were adjusted from one run to the next by the conventional means of scaling all momenta uniformly.

Table II presents results computed for a set of nine distinct temperatures. For each of these nine states the system was equilibrated for $4000\Delta t^*=20$ reduced time units, then the requisite averages were formed over the subsequent $12\,000\Delta t^*=60$ reduced time units. In none of the cases could we detect symptoms of disequilibrium over the averaging period.

In addition to the previously discussed quantities ϕ and p_{ex}, Table II also provides values found for $g(0)$, the pair-correlation function evaluated at zero separation. This quantity vividly conveys the extent to which particles are able to interpenetrate. In the extreme high-temperature limit the Gaussian core potential Φ is incapable of perturbing the system-configuration ensemble from that of an ideal gas, and $g(r)$ would be identically unity for all r. The extent to which $g(0)$ deviates from unity thus provides a convenient measure of configurational nonideality.

The high-temperature limits for ϕ and for p_{ex} are easily found to be

$$\lim_{\beta\to 0}\phi(\beta)=0.906\,899\,6821 ,$$
$$\lim_{\beta\to 0}p_{\mathrm{ex}}(\beta)=0.523\,598\,7756 . \tag{3.2}$$

Figures 3 and 4 show the molecular-dynamics results for ϕ and p_{ex} as inverted triangles. It should be stressed that the range shown in these figures is indeed the high-temperature regime, since the freezing transition is encountered only when β increases to approximately 138.9.

IV. DISCUSSION

Direct calculation shows that the first few terms from asymptotic series (2.3) and (2.4), regarded sim-

TABLE II. Molecular-dynamics simulation data.

β	ϕ	p_{ex}	$g(0)$
0.099 261	0.864 127 2150	0.511 351 483	0.888
0.222 14	0.824 040 1235	0.501 138 898	0.805
0.495 05	0.770 874 0256	0.488 192 466	0.705
1.070 4	0.696 549 4077	0.473 399 342	0.487
2.222 0	0.623 257 9440	0.463 012 300	0.340
4.345 6	0.560 219 7513	0.462 061 942	0.156
7.985 3	0.512 172 1722	0.464 502 106	0.043
14.110	0.478 612 8133	0.471 014 572	0.008
24.415	0.455 780 8906	0.477 523 632	0.001

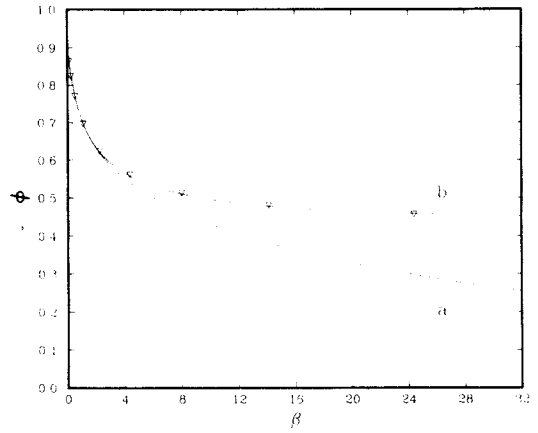

FIG. 3. Potential energy per particle for the two-dimensional Gaussian core model at reduced density $3^{-1/2}$. Molecular-dynamics data are shown as inverted triangles. Curve *a*, four-term approximant; curve *b*, five-term approximant.

ply as polynomial approximants to ϕ and p_{ex}, are incapable of reproducing even the qualitative behavior of the data in Figs. 3 and 4. This confers additional importance on the Borel transforms as means of simply fitting the data to closed-form functions. We now attempt to illustrate the possibilities for such fitting in the light of results obtained in Sec. II.

Recalling the conclusion that $G(x)$ and $H(x)$ were analytic throughout the complex plane, it seems reasonable to represent these functions approximately as finite sums of exponentials:

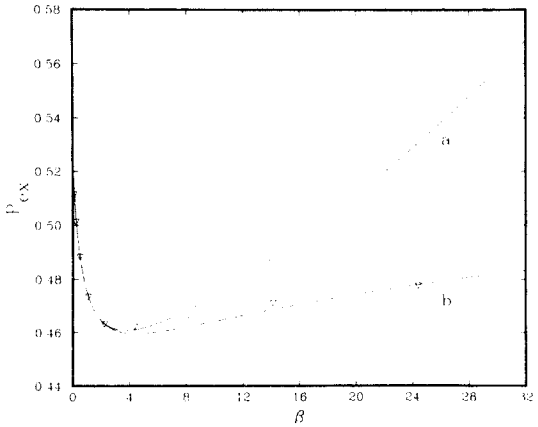

FIG. 4. Excess pressure for the two-dimensional Gaussian core model at reduced density $3^{-1/2}$. Molecular-dynamics data are shown as inverted triangles. Curve *a*, four-term approximant; curve *b*, five-term approximant.

$$G(x)\simeq\sum_{j=1}^{n} G_j\exp(-\gamma_j x)\ ,$$

$$H(x)\simeq\sum_{j=1}^{n} H_j\exp(-\eta_j x)\ . \tag{4.1}$$

The constants G_j, γ_j, H_j, and η_j could be chosen to reproduce power-series expansions (2.7) through any given order. Equations (4.1) then imply

$$\phi(\beta)\simeq\sum_{j=1}^{n} G_j/(1+\gamma_j\beta)\ ,$$

$$p_{ex}\simeq\pi^{-D/2}\rho_D\sum_{j=1}^{n} H_j/(1+\eta_j\beta)\ . \tag{4.2}$$

As more and more exponentials are used to improve the representations of G and H, it is presumably the case that the β-plane poles appearing in Eqs. (4.2) will become densely arrayed along the negative axis to simulate branch cuts. Furthermore, we would expect that the series of simple exponential functions (4.1) should converge to limits consistent with the asymptotic forms (2.24) and (2.29).

The sets of eight series coefficients shown in Table I suffice to determine four-term approximants to G and H of type (4.1). We have calculated the corresponding constants G_j, γ_j, H_j, and η_j with numerical results collected in Table III. The implied approximations for ϕ and p_{ex} were then computed, and are shown in Figs. 3 and 4 as curves labeled *a*. Overall these curves have qualitatively the proper behavior indicated earlier by the simulation data. In particular, the very interesting minimum in p_{ex} appears once again. Nevertheless there still remain quantitative deficiencies; in particular, the four-exponential approximant for G yields ϕ values that are clearly too low for β greater than about 4.

If more series coefficients were available beyond those shown in Table I the corresponding approximants no doubt would do a better job of reproducing the simulation data. Because higher-order series coefficients are not yet known, an interim alternative is to appeal to the simulation data itself to suggest improvements. In particular, we take note of the fact that ϕ and p_{ex} in the simulations[3,4,6] are

TABLE III. Parameters for four-exponential Borel approximants.

j	G_j	γ_j	H_j	η_j
1	0.566 737	0.040 933	0.750 095	−0.007 361
2	0.254 552	0.892 689	0.111 871	1.073 311
3	0.078 568	2.249 352	0.041 144	2.376 888
4	0.007 042	3.733 180	0.003 790	3.794 451

TABLE IV. Parameters for five-exponential Borel approximants. The terms for $j=0$ were "forced" into the approximants to improve fits to molecular-dynamics data.

j	G_j	γ_j	H_j	η_j
0	0.416 000	−0.000 500	0.859 097	−0.000 500
1	0.215 575	0.273 919	−0.111 346	0.056 619
2	0.203 841	1.064 427	0.113 139	1.054 491
3	0.065 674	2.368 688	0.042 107	2.360 369
4	0.005 810	3.799 189	0.003 902	3.784 525

roughly constant over the wide β range from 32 (the largest value shown in Figs. 3 and 4) to the freezing-point value 138.9. Such behavior could only arise from one or more terms in Eqs. (4.1) and (4.2) having very small exponential decay constants γ_j and η_j. By simple numerical experimentation we have found that if G and H incorporate fifth exponentials with constants

$$\gamma_0=\eta_0=-0.0005\ ,$$
$$G_0=0.416\,000\ , \tag{4.3}$$
$$H_0=0.859\,057\ ,$$

then the simulation data can be more closely fitted. By forcing these new terms into the Borel transforms G and H the remaining exponentials require shifted parameters to continue fitting the power-series coefficients listed in Table I. Table IV shows the sets of ten parameters required for these five-exponential approximants. Curves labeled b in Figs. 3 and 4 display the resulting predictions for ϕ and p_{ex}. While these predictions are still imperfect, improvement is clear, particularly for ϕ.

We believe it is significant that the additional functions forced into G and H so as to improve large-β predictions are automatically found to increase exponentially with variable x. Evidently the transforms have begun to exhibit crudely the kind of asymptotic behavior adduced in Sec. II. The exponential rise rate is not correct, of course, but it is small, as required, and would probably improve if yet further terms could be incorporated. This rough indication that the proper behavior of G and H along the positive real axis has begun to emerge confers extra importance on the task of generating further exact series coefficients for the model.

[1]J. E. Mayer and M. G. Mayer, *Statistical Mechanics* (Wiley, New York, 1940), Chap. 13.

[2]A. A. Maradudin, E. W. Montroll, G. H. Weiss, and I. P. Ipatova, *Theory of Lattice Dynamics in the Harmonic Approximation,* 2nd ed. (Academic, New York, 1971).

[3]F. H. Stillinger and T. A. Weber, J. Chem. Phys. 74, 4015 (1981).

[4]T. A. Weber and F. H. Stillinger, J. Chem. Phys. 74, 4020 (1981).

[5]F. H. Stillinger, J. Chem. Phys. 65, 3968 (1976).

[6]F. H. Stillinger and T. A. Weber, Phys. Rev. A 25, 978 (1982).

[7]F. H. Stillinger, Phys. Rev. B 20, 299 (1979).

[8]F. H. Stillinger, J. Chem. Phys. 70, 4067 (1979).

[9]R. C. Buck, *Advanced Calculus,* 2nd ed. (McGraw-Hill, New York, 1965), p. 161.

[10]J. P. McTague, D. Frenkel, and M. P. Allen, in *Ordering in Two Dimensions,* edited by S. K. Sinha (Elsevier and North-Holland, New York, 1980), pp. 147–151.

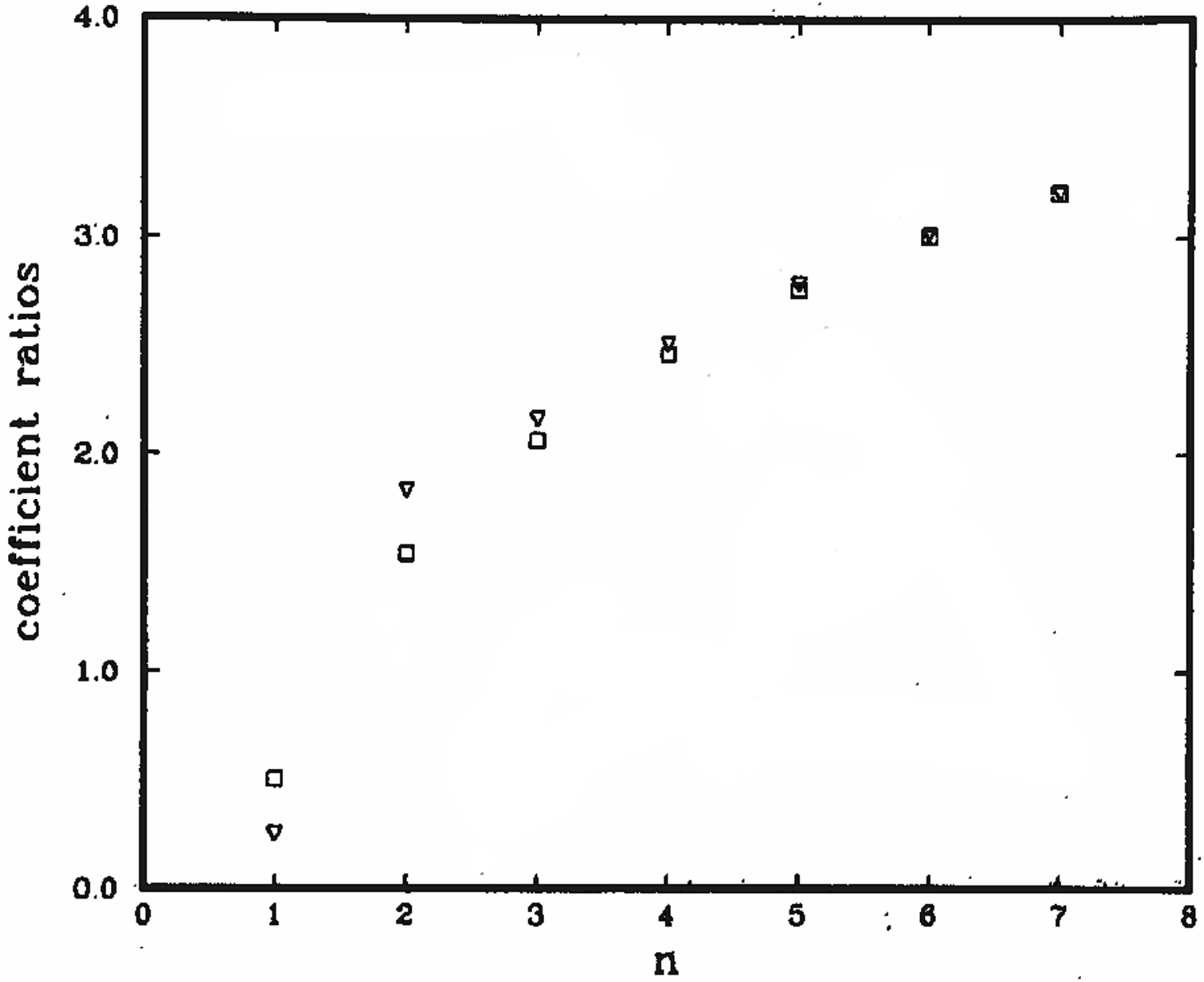

FIG. 1. Ratios of successive series coefficients plotted against order n. Squares show A_n/A_{n-1} from Eq. (2.3) and the inverted triangles show C_n/C_{n-1} from Eq. (2.4).

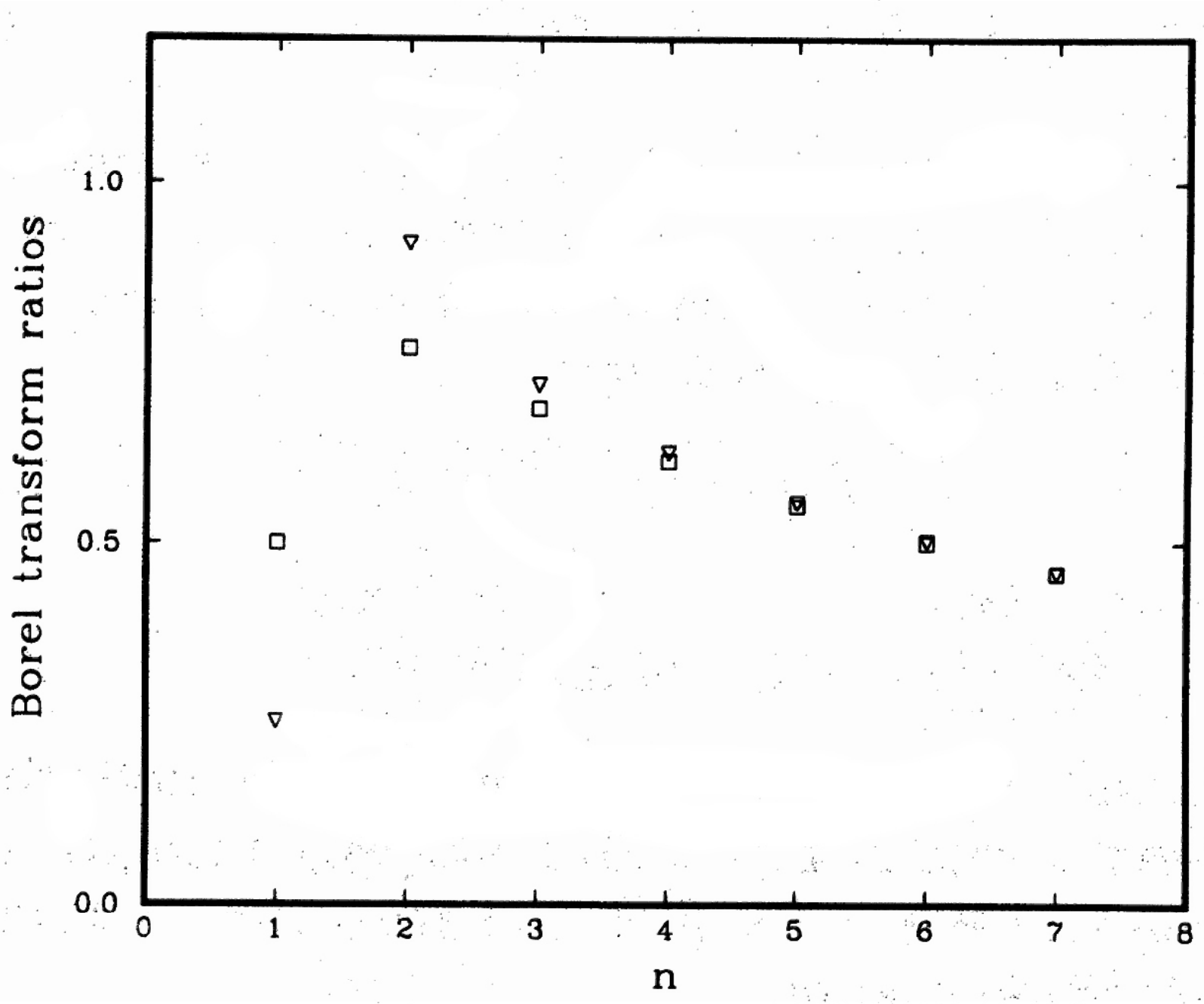

FIG. 2. Series-coefficient ratios for Borel transforms. Squares refer to G defined in Eq. (2.5), inverted triangles refer to H defined in Eq. (2.6).

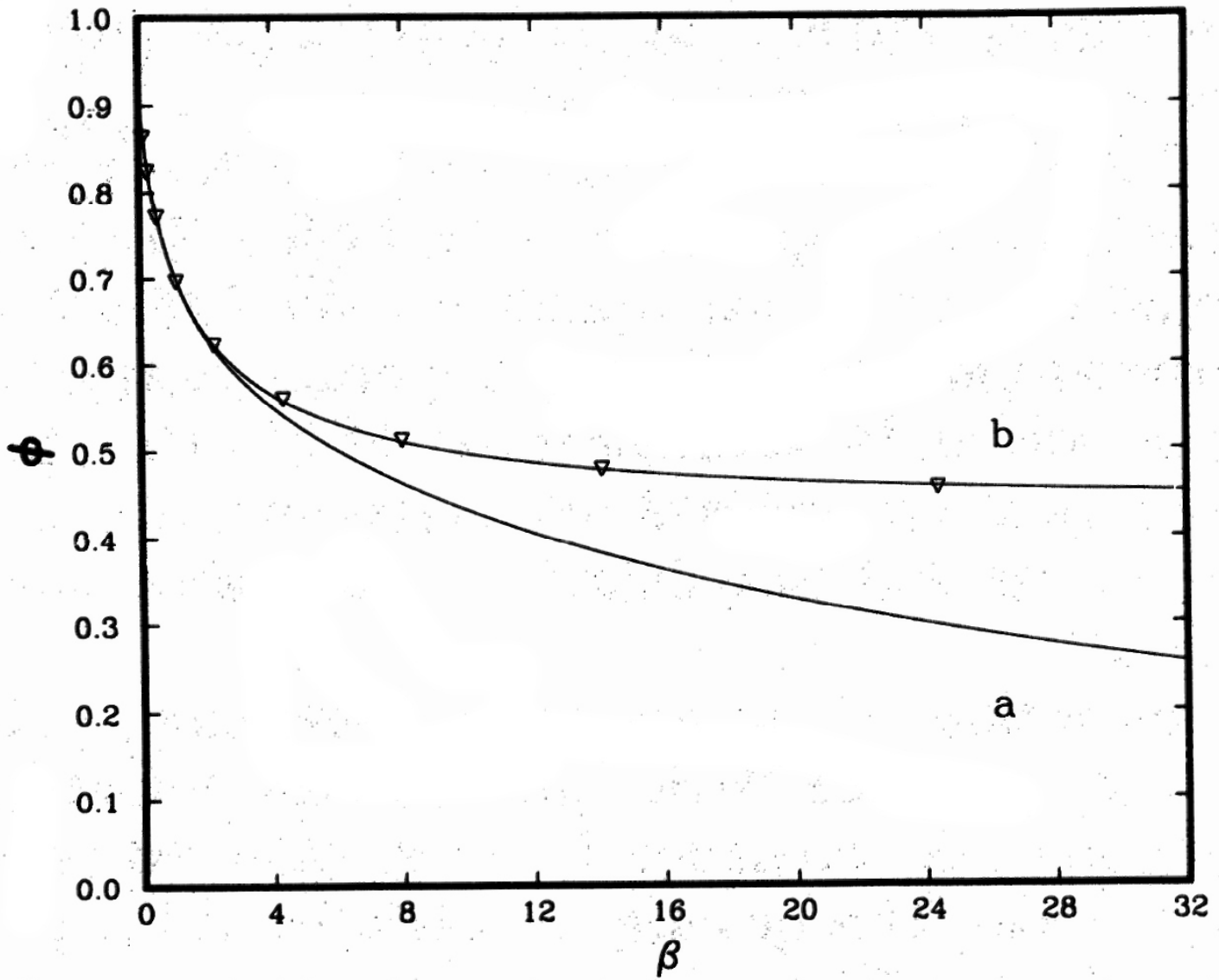

FIG. 3. Potential energy per particle for the two-dimensional Gaussian core model at reduced density $3^{-1/2}$. Molecular-dynamics data are shown as inverted triangles. Curve *a*, four-term approximant; curve *b*, five-term approximant.

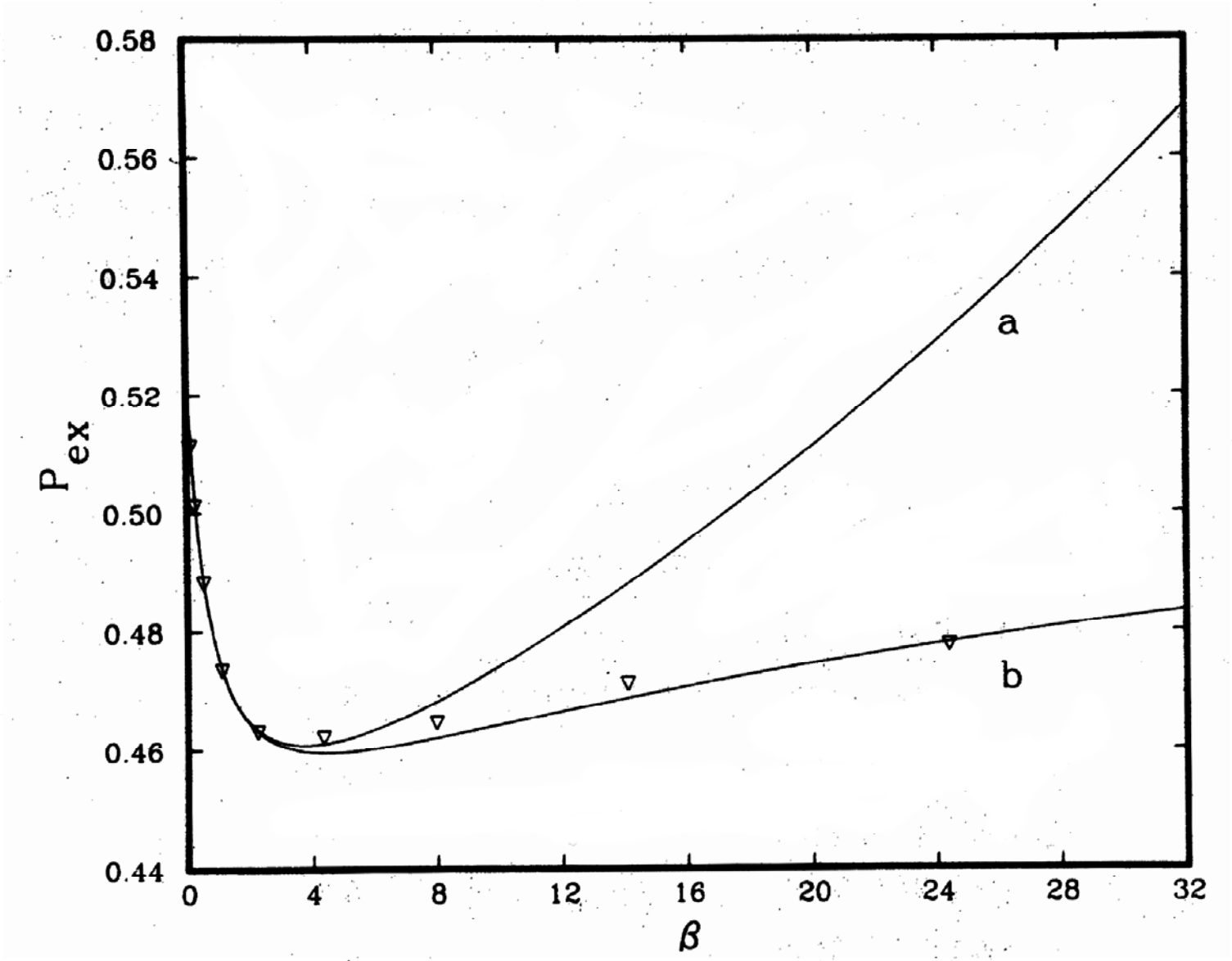

FIG. 4. Excess pressure for the two-dimensional Gaussian core model at reduced density $3^{-1/2}$. Molecular-dynamics data are shown as inverted triangles. Curve *a*, four-term approximant; curve *b*, five-term approximant.